Available online at www.sciencedirect.com
ScienceDirect
Journal of Sound and Vibration 298 (2006) 907–917
JOURNAL OF SOUND AND VIBRATION
www.elsevier.com/locate/jsvi

Experimental verification of Jeffcott rotor model with preloaded snubber ring

E.V. Karpenko, M. Wiercigroch*, E.E. Pavlovskaia, R.D. Neilson

Centre for Applied Dynamics Research, Department of Engineering, University of Aberdeen, King's College, Aberdeen AB24 3UE, UK

Received 7 October 2004; received in revised form 17 May 2006; accepted 30 May 2006
Available online 23 August 2006

Abstract

This paper describes the experimental verification of a nonlinear Jeffcott rotor model with a preloaded snubber ring. The nonlinearity, in the form of a discontinuous stiffness, is caused by the radial clearance between rotor and the snubber ring. The rotor is placed eccentrically within the snubber ring and the eccentricity can be varied. For purpose of clarity the mathematical model of the rotor system with the preloaded snubber ring developed in Pavlovskaia et al. [Nonlinear dynamics of a Jeffcott rotor with a preloaded snubber ring, *Journal of Sound and Vibration* 276 (2004) 361–379] is presented briefly. Theoretical results obtained from analytical approximate solutions and numerical simulations of the model are verified by the experimental study. A detailed description of the experimental rig and the data acquisition system developed are presented, along with the experimental procedures used to investigate the dynamical responses of the system. The results concentrate on the dynamic responses caused by interactions between the whirling rotor and the massless snubber ring, which has much higher support stiffness than the rotor. Bifurcation diagrams, Poincaré maps and phase plane diagrams are used to compare the results obtained from the experiment and the theory. Good correlation between the experimental and theoretical results is found.

1. Introduction

In rotor systems complex behaviour may occur due to various nonlinear effects of different types and strength. One of the most interesting and practically important dynamic responses of rotor systems are caused by bearing clearances, which are mainly due to piecewise nature of stiffness characteristics. It is well known that dynamic interactions in such systems can lead to much more complex nonlinear behaviour than in systems with smooth nonlinearities [1,2], including existence of grazing bifurcations and untypical routes to chaos such blowout. In rotor systems, such phenomena are caused by intermittent contacts between the components of the rotor system, which can lead to catastrophic failures. Therefore, it is vastly important to conduct experimental verifications in order establish credible mathematical models predicting complex dynamic responses of rotor systems.

*Corresponding author. Tel.: +44 1224 272509; fax: +44 1224 272497.
E-mail address: M.Wiercigroch@eng.abdn.ac.uk (M. Wiercigroch).

0022-460X/$ - see front matter © 2006 Elsevier Ltd. All rights reserved.
doi:10.1016/j.jsv.2006.05.044

Nomenclature

c_r	damping coefficient of the rotor
c_s	damping coefficient of the snubber ring
D	distance between the centres of the rotor and the snubber ring
f	forcing frequency
k_r	rotor stiffness
k_s	snubber ring stiffness
M	mass of rotor
$m\rho$	out-of-balance
R	radial displacement of the rotor relative to the initial position of the snubber ring
x_r	displacement of the rotor in the horizontal direction relative to the initial position of the snubber ring
y_r	displacement of the rotor in the vertical direction relative to the initial position of the snubber ring
x_s	displacement of the snubber ring in the horizontal direction
y_s	displacement of the snubber ring in the vertical direction

Greek letters

Δ_x	preloading of the snubber ring in the horizontal direction
Δ_y	preloading of the snubber ring in the vertical direction
ε_x	eccentricity of rotor in the x-direction
ε_y	eccentricity of rotor in the y-direction
φ_0	initial phase shift

Rotor systems with bearing clearances have been studied in the past, where the investigations concentrated primarily on the Jeffcott rotors. In particular, Choy and Padovan [3], Muszynska and Goldman [4], Childs [5] and Chu and Zhang [6,7] paid attention to rub interactions in rotating machinery. Ehrich [8] investigated spontaneous sidebanding, while Ganesan [9] looked at the stability analysis. Synchronous and subharmonic responses were also investigated in Refs. [5,10–12]. Numerical investigation of the Jeffcott rotor model with a snubber ring by Karpenko et al. [13] has shown the existence of multiple attractors and fractal basins of attraction. Influence of the preloading and viscous damping of the snubber ring was investigated in Ref. [14] where it was shown how the preloading could stabilize the dynamic response. Gonsalves et al. [15] designed an experimental rig to simulate the Jeffcott model and made a preliminary comparative analysis between the experimental and numerical results.

Chaotic behaviour of a simple model of a Jeffcott rotor, supported hydrodynamically using short bearing theory was considered by Brown et al. [16,17]. In Ref. [17] it was demonstrated that the system behaved chaotically when the rotating unbalance force exceeded the gravitational load. They showed that at these values of the force ratio the time history of the response is very sensitive to initial conditions and a spectral analysis demonstrates a significant broadening from the expected peak at the rotational frequency.

The present paper complements our earlier studies presented in Refs. [13–15] by an experimental verification of the theoretical predictions obtained using the model developed in Ref. [18]. Data from our experimental rig has been collected and processed using a LabView data acquisition system, which allows the generation of bifurcation diagrams and Poincaré maps and also to review on-line the system responses in the form of the phase planes and time histories. In this paper, attention is paid to how the dynamics of the Jeffcott rotor depend on the system and control parameters, in particular the shaft rotational speed (excitation frequency). Diagrams were constructed for different eccentricities and preloading.

The main aims of this work are (i) to assess the correlation between the responses from the new theoretical model of the rotor system [18] with the experiments, and (ii) to obtain an overview of the global system dynamics, which can be consequently used to suppress the rotor vibration.

2. Experimental set-up

Fig. 1 shows the rotor rig which comprises essentially two main parts, a rigid rotor (1), visco-elastically supported by four flexural rods (2) and excited by the out-of-balance mass (3), and a snubber ring (4) also elastically supported by four compression springs. The rotor assembly consists of a steel rotor, running in two angular contact bearings. Lightly preloaded angular contact bearings are used to ensure there is no axial

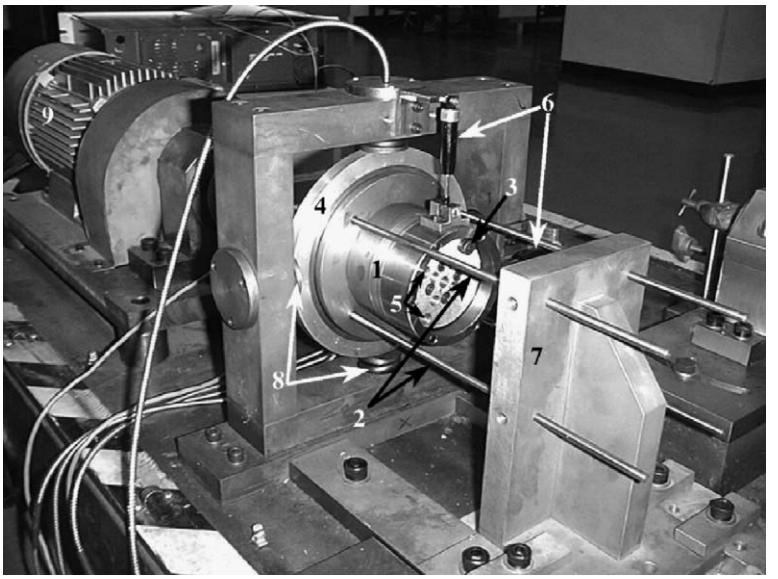

Fig. 1. Photograph of the experimental Jeffcott rotor.

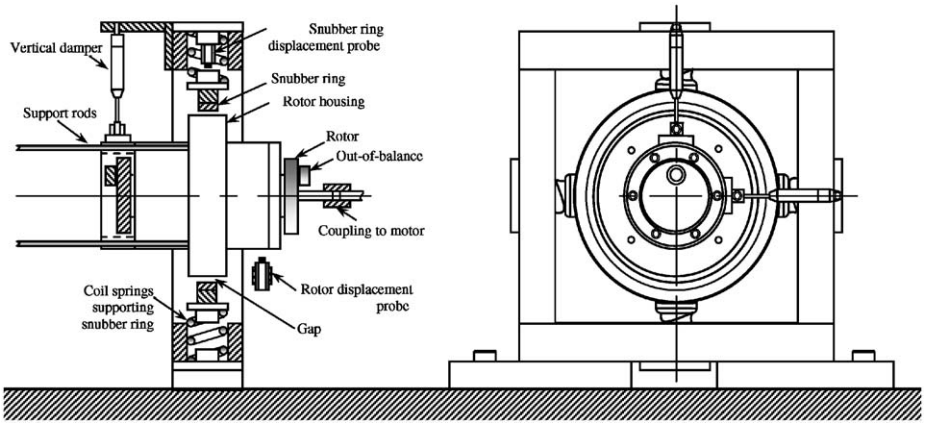

Fig. 2. Design drawing of experimental set-up.

movement. Inner sleeves were fastened to the rotor to hold the bearings in place and oil seals were fitted. Holes (5) were drilled and tapped in both inner sleeves for the addition of imbalance weights. A pair of dampers (6) was attached to the rotor, one in each direction, to provide the system with heavier damping. The damping is assumed to be linear viscous.

Four flexural rods (2) are clamped symmetrically at one end to the outer bearing housing and at the other to a large support block. The support block (7) is in turn bolted to a large cast iron bed. The discontinuous stiffness is provided by a ring to which four compression springs (8), of much greater stiffness than that of the flexural rods, are secured symmetrically. The other ends of the springs are fixed to a large frame, clamped to the bed. The rotor runs inside the ring, with a radial clearance between the ring (4) and the outer bearing housing (1). Two different outer rings were used in the experiments one with a 0.5 mm gap and another with 0.75 mm. The design drawings of the experimental set-up are presented in Fig. 2.

The rotor is driven by a variable speed DC motor (9) controlled by a single-phase thyristor controller, which features a closed-loop feedback using a tacho-generator. Utilizing a Fenner-type coupling, the drive shaft of the motor is connected to a drive block employed to reduce the size of the drive shaft from the motor and to mount the shaft speed monitoring disc. The shaft speed monitoring disc has a notch cut into it, which is

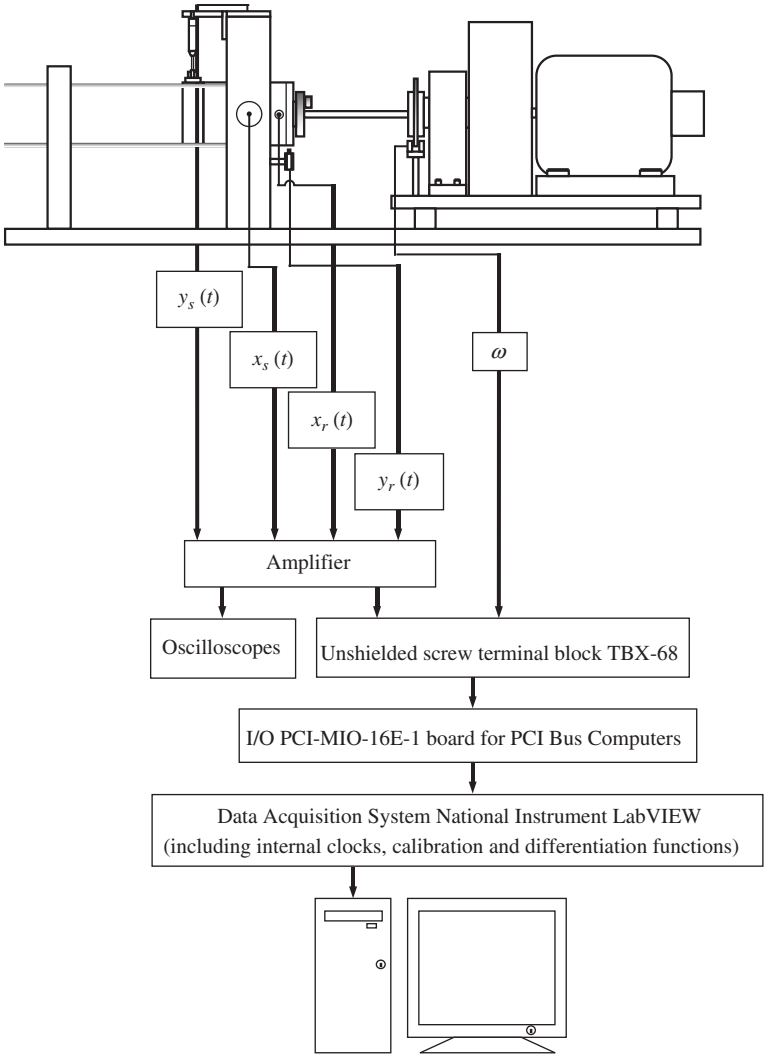

Fig. 3. Schematic of instrumentation layout.

aligned with the imbalance mass. As the notch passes a light-emitting-diode optoswitch, a once-per-revolution phase signal is obtained. The displacements of the rotor system are monitored by noncontacting eddy probes. Two probes were used for the rotor and another two for the snubber ring (see Fig. 2(a) and also the flow diagram for instrumentation in Fig. 3). Subsequently, the displacement and forcing frequency signals were collected by an unshielded screw terminal block TBX-68 supplier and then handled in a PCI-MIO-16E-1 A/D board and transferred to the National Instrument data acquisition system LabView, using a purpose-written program on a PC controlling the rate of sampling, the number of samples, calibration and computation of the rotational frequency. The relative velocities of the rotor and the snubber ring $\dot{x}_r$, $\dot{y}_r$, $\dot{x}_s$ and $\dot{y}_s$ were calculated using the LabView digital differentiation facility applied to the output signals from the eddy current probes. The data was collated on the computer, where it was scaled, plotted and analysed in the form of Poincaré maps and bifurcation diagrams.

3. Experimental verification of mathematical model of Jeffcott rotor with preloaded snubber ring

The experimental rig shown in Fig. 1 is modelled as a two-degrees-of-freedom piecewise nonlinear planar oscillator, where the rotor makes intermittent contact with the preloaded snubber ring. As mentioned earlier

the mathematical model for this system has been developed in Ref. [18], however for the purpose of clarity and relevance to the mathematical predictions presented later, a brief summary is given below. In addition, we have adopted in this paper the dimensional formulation of the mathematical model for the sake of clarity and simplicity when comparing the theoretical predictions with the experimental results.

The physical model and its geometrical description are given in Fig. 4. The excitation of the rotor is provided by an out-of-balance rotating mass producing the loading force of $m\rho\omega^2$. Here O_r and O_s denote the current positions of the rotor and the snubber ring, respectively. Fig. 4(a) presents the situation when the initial and current positions of the snubber ring coincide. The eccentricity vector $\boldsymbol{\varepsilon} = (\varepsilon_x, \varepsilon_y)$ determines the initial position of the rotor $O_{r,0}$ relative to the initial position of the outer ring. In Fig. 4(a) the initial location of the rotor in respect of the $\boldsymbol{\varepsilon}$ is shown by dash line. The radius vectors $\mathbf{R}_s$ and $\mathbf{R}_r$ show the current positions of the rotor and the snubber ring. The term $D = \sqrt{(x_r - x_s)^2 + (y_r - y_s)^2}$ is the distance between the centres of the rotor and the snubber ring. $R = \sqrt{x_r^2 + y_r^2}$ is the radial displacement of the rotor. For the "no contact" situation the distance between the centres of the rotor and the snubber ring is equal to the radial displacement of the rotor $D = R$. To derive the equations of motion the absolute coordinate system (x, y), shown in Fig. 4(b), was chosen. When rotor moves inside the stator without any interaction with the ring the equations of motion for the rotor and the snubber ring are as follows

$$\begin{aligned} &M\ddot{x}_r + c_{r_x}\dot{x}_r + k_{r_x}(x_r - \varepsilon_x) = m\rho\omega^2 \cos(\varphi_0 + \omega t),\\ &M\ddot{y}_r + c_{r_y}\dot{y}_r + k_{r_y}(y_r - \varepsilon_y) = m\rho\omega^2 \sin(\varphi_0 + \omega t),\\ &k_s x_s + c_s\dot{x}_s = 0,\\ &k_s y_s + c_s\dot{y}_s = 0. \end{aligned} \tag{1}$$

When the rotor is in contact with the snubber ring there are four unique regimes, for which the stiffness of the snubber ring for x and y directions differs.

1. The displacement of the snubber ring greater than the preloading

$$\begin{aligned} &|x_s| > \Delta_x,\ |y_s| > \Delta_y,\\ &M\ddot{x}_r + c_{r_x}\dot{x}_r + c_s\dot{x}_s + k_{r_x}(x_r - \varepsilon_x) + k_s x_s = m\rho\omega^2 \cos(\varphi_0 + \omega t),\\ &M\ddot{y}_r + c_{r_y}\dot{y}_r + c_s\dot{y}_s + k_{r_y}(y_r - \varepsilon_y) + k_s y_s = m\rho\omega^2 \sin(\varphi_0 + \omega t). \end{aligned} \tag{2}$$

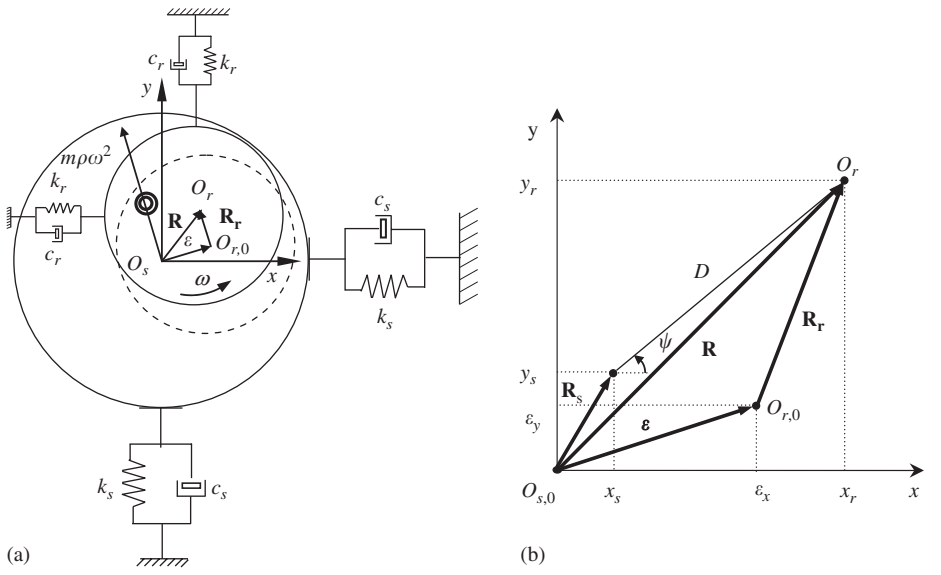

Fig. 4. (a) Physical model and (b) coordinate system.

2. The displacement of the snubber ring is greater than the preloading in y direction

$$|x_s| \le \Delta_x \text{ and } |y_s| > \Delta_y,$$
$$M\ddot{x}_r + c_{r_x}\dot{x}_r + 2c_s\dot{x}_s + k_{r_x}(x_r - \varepsilon_x) + 2k_s x_s = m\rho\omega^2 \cos(\varphi_0 + \omega t),$$
$$M\ddot{y}_r + c_{r_y}\dot{y}_r + c_s\dot{y}_s + k_{r_y}(y_r - \varepsilon_y) + k_s y_s = m\rho\omega^2 \sin(\varphi_0 + \omega t). \quad (3)$$

3. The displacement of the snubber ring is greater than the preloading in x direction

$$|x_s| > \Delta_x \text{ and } |y_s| \le \Delta_y,$$
$$M\ddot{x}_r + c_{r_x}\dot{x}_r + c_s\dot{x}_s + k_{r_x}(x_r - \varepsilon_x) + k_s x_s = m\rho\omega^2 \cos(\varphi_0 + \omega t),$$
$$M\ddot{y}_r + c_{r_y}\dot{y}_r + 2c_s\dot{y}_s + k_{r_y}(y_r - \varepsilon_y) + 2k_s y_s = m\rho\omega^2 \sin(\varphi_0 + \omega t). \quad (4)$$

4. The preloading acts in both directions

$$|x_s| \le \Delta_x \text{ and } |y_s| \le \Delta_y,$$
$$M\ddot{x}_r + c_{r_x}\dot{x}_r + 2c_s\dot{x}_s + k_{r_x}(x_r - \varepsilon_x) + 2k_s x_s = m\rho\omega^2 \cos(\varphi_0 + \omega t),$$
$$M\ddot{y}_r + c_{r_y}\dot{y}_r + 2c_s\dot{y}_s + k_{r_y}(y_r - \varepsilon_y) + 2k_s y_s = m\rho\omega^2 \sin(\varphi_0 + \omega t). \quad (5)$$

In Eqs. (1)–(5) M and m are the mass of the rotor, and the imbalance, respectively, k_{r_x} and c_{r_x} and k_{r_y} and c_{r_y} denote the stiffness and the viscous damping of the rotor in the x- and y-directions, k_s and c_s are the stiffness and viscous damping of the snubber ring, ω is the rotation frequency, and φ_0 is the initial phase shift. The distance from the centre of rotation to the location of the mass imbalance, m, is defined by ρ. For Eqs. (2)–(5) the constraints between the rotor and the snubber ring coordinates were developed in [18] and are listed in Table 1.

Equations of motion (1)–(5) have been derived using the following series of assumptions. Firstly, dry friction between the ring and rotor has been neglected. Secondly, it was assumed that the snubber ring itself is massless, because it is manufactured from aluminium and highly preloaded by compression springs. Thirdly, gyroscopic forces are not taken into consideration since no angular motion of the rotor axis O_r occurs.

A sample of extensive experimental studies [19] conducted to verify the mathematical model of Jeffcott rotor system with a preloaded snubber ring developed at the University of Aberdeen [18] is presented here. The following values of the system parameters were chosen: the rotor mass and mass of the out-of-balance were $M = 9.7\,\text{kg}$ and $m = 0.028\,\text{kg}$, respectively. The combined stiffness of the rods supporting the rotor was $k_{r_x} = k_{r_y} = 79\,\text{kN/m}$; this yields a natural frequency of 14.4 Hz. The snubber ring stiffness was $k_s = 2354\,\text{kN/m}$. The equivalent viscous damping from the rods and the dampers in the horizontal and vertical directions was the same equal to $c_{r_x} = c_{r_y} = 105\,\text{kg/s}$. The out-of-balance radius, was $\rho = 35\,\text{mm}$.

For the bifurcation diagrams, the forcing frequency (the shaft rotational speed) was varied from 7 to 30 Hz and for some tests up to 50 Hz to examine the global bifurcations. The system responses were investigated by collecting data with forcing frequency steps of around 0.6–1 Hz. The continuation method was applied, so for

Table 1
Relationships between the rotor and the snubber ring coordinates

$x_s(x_r, y_r)$	$y_s(x_r, y_r)$	Snubber ring location
$x_s = x_r\left(\sqrt{x_r^2 + y_r^2} - \gamma\right)/\sqrt{x_r^2 + y_r^2}$	$y_s = y_r\left(\sqrt{x_r^2 + y_r^2} - \gamma\right)/\sqrt{x_r^2 + y_r^2}$	$\lvert x_s\rvert < \Delta_x,\ \lvert y_s\rvert < \Delta_y$
$x_s = \frac{2y_s(x_r + \Delta_x \operatorname{sgn}(x_s))}{y_r + y_s} - \Delta_x \operatorname{sgn}(x_r)$	$(y_r - y_s)^2\left((x_r + \Delta_x \operatorname{sgn}(x_s))^2 + (y_r + y_s)^2\right) = \gamma^2(y_r + y_s)^2$	$\lvert x_s\rvert \ge \Delta_x,\ \lvert y_s\rvert < \Delta_y$
$(x_r - x_s)^2\left((y_r + \Delta_y \operatorname{sgn}(y_s))^2 + (x_r + x_s)^2\right) = \gamma^2(x_r + x_s)^2$	$y_s = \frac{2x_s(y_r + \Delta_y \operatorname{sgn}(y_s))}{x_r + x_s} - \Delta_y \operatorname{sgn}(y_s)$	$\lvert x_s\rvert < \Delta_x,\ \lvert y_s\rvert \ge \Delta_y$
$x_s = \frac{(x_r + \Delta_x \operatorname{sgn}(x_s))(\tilde{R} - \gamma)}{\tilde{R}} - \Delta_x \operatorname{sgn}(x_s),$ $\tilde{R} = \sqrt{(x_r + \Delta_x \operatorname{sgn}(x_s))^2 + (y_r + \Delta_y \operatorname{sgn}(y_s))^2}$	$y_s = \frac{(y_r + \Delta_y \operatorname{sgn}(y_s))(\tilde{R} - \gamma)}{\tilde{R}} - \Delta_y \operatorname{sgn}(y_s)$	$\lvert x_s\rvert \ge \Delta_x,\ \lvert y_s\rvert \ge \Delta_y$

each frequency the initial conditions were taken from the previous examined frequency discarding about 400 cycles in order to ensure that steady-state behaviour is reached.

For the bifurcation diagram presented in Fig. 5 a comparison of the theoretical (Fig. 5a) and experimental (Fig. 5b) responses shows a good degree of similarity. In both figures for the low magnitude of the forcing frequency period one motion is observed for $f \in (7, 13.6)$ Hz and for $f \in (16.2, 17.7)$ Hz followed by chaotic regimes for $f \in (13.6, 16.2)$ Hz and $f \in (17.7, 22.8)$ Hz, respectively. In the theoretical and experimental diagrams the width of both periodic and chaotic regimes are the same. After the flip bifurcation at $f \approx 22.8$ Hz the theoretical response becomes periodic up to the end of the diagram. In the experimental bifurcation diagram in Fig. 5(b) at $f \in (25.6, 32)$ Hz a quasi-periodic regime was obtained. In both diagrams two cross-sections were examined in more detail by constructing Poincaré maps. Here chaotic attractors were obtained for: $f = 14.4$ and 19.3 Hz keeping the remaining parameters constant: $k_s = 2354\,\mathrm{kN/m}$, $k_{r_x} = k_{r_y} = 79\,\mathrm{kN/m}$, $c_{r_x} = c_{r_y} = 105\,\mathrm{kg/s}$, $M = 9.7\,\mathrm{kg}$, $m = 0.028\,\mathrm{kg}$, $\rho = 35\,\mathrm{mm}$, $\gamma = 0.5\,\mathrm{mm}$, $\varepsilon_x = 0.025\,\mathrm{mm}$, $\varepsilon_y = 0.20\,\mathrm{mm}$

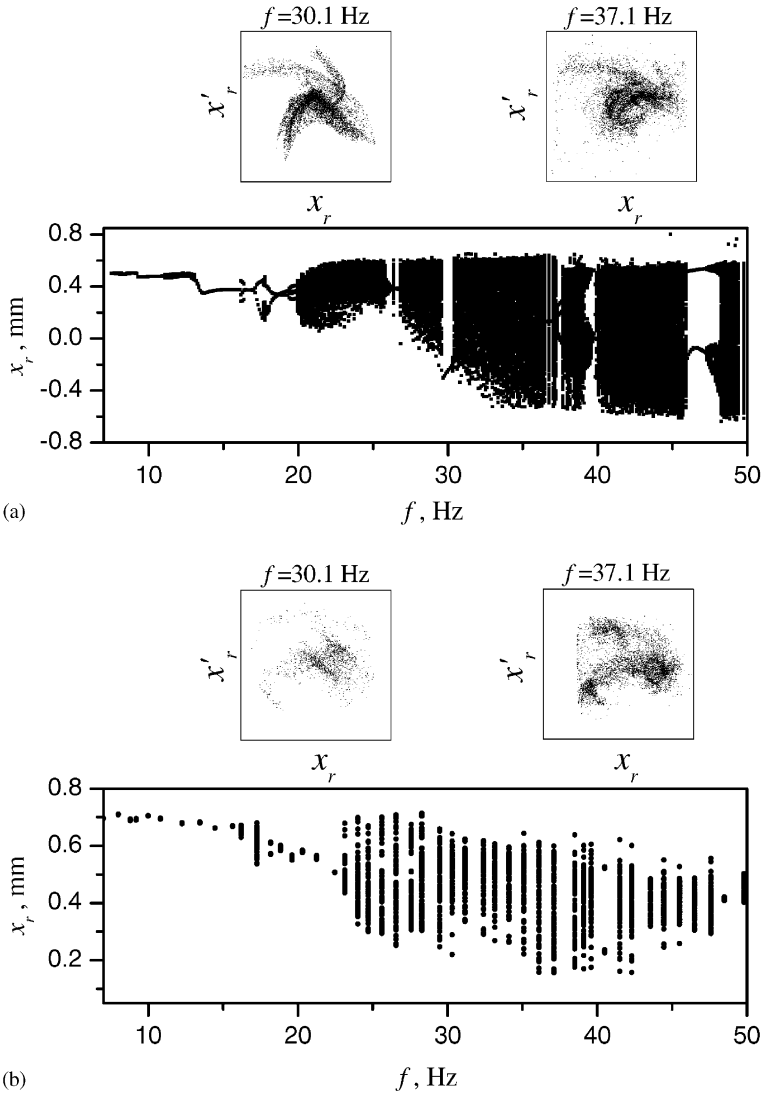

Fig. 5. Bifurcation diagram for the forcing frequency where $k_s = 2354\,\mathrm{kN/m}$, $k_{r_x} = k_{r_y} = 79\,\mathrm{kN/m}$, $c_{r_x} = c_{r_y} = 105\,\mathrm{kg/s}$, $c_s = 3.5\,\mathrm{kg/s}$, $M = 9.7\,\mathrm{kg}$, $m = 0.028\,\mathrm{kg}$, $\rho = 35\,\mathrm{mm}$, $\gamma = 0.5\,\mathrm{mm}$, $\varepsilon_x = 0.025\,\mathrm{mm}$, $\varepsilon_y = 0.20\,\mathrm{mm}$ and $\Delta_x = \Delta_y = 0.04\,\mathrm{mm}$; (a) theoretical and (b) experimental.

and $\Delta_x = \Delta_y = 0.04$ mm. It is apparent that the theoretical and experimental attractors are similar in shape. Despite the similarity of shape, there are some differences in the amplitudes of displacements and velocities.

In the next experiment the eccentricity ratios were set up as $\varepsilon_x = 0.45$ mm and $\varepsilon_y = 0.05$ mm. The bifurcation diagrams constructed theoretically and experimentally for this case are presented in Fig. 6. Because only period one motion regime exists in the interval $f \in (30, 50)$ Hz, the maximum forcing frequency for these diagrams was reduced to 30 Hz. Comparing with the previously shown diagrams of Fig. 5, here the eccentricity change leads to aggregation of two chaotic zones into one, and the transition from period one motion to chaos now is carried out through period doubling bifurcations. The experimental result of Fig. 6(b) follows all the basic bifurcations observed theoretically such as the period doubling bifurcation at $f \approx 14.74$ Hz and the flip bifurcation at $f \approx 26.1$ Hz. Phase portraits for the periodic and chaotic cross-sections were plotted for $f = 17.6$ and 25 Hz showing also a good correspondence.

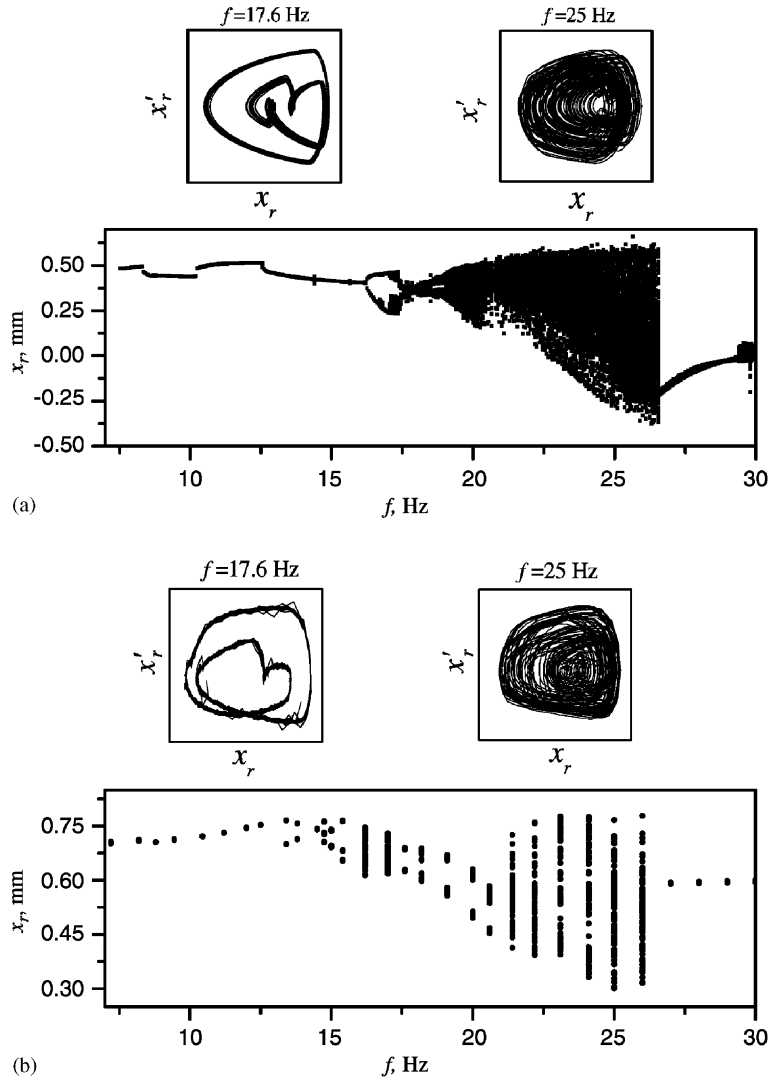

Fig. 6. Bifurcation diagram for the forcing frequency where $k_s = 2354$ kN/m, $k_{rx} = k_{ry} = 79$ kN/m, $c_{rx} = c_{ry} = 105$ kg/s, $c_s = 3.5$ kg/s, $M = 9.7$ kg, $m = 0.028$ kg, $\rho = 35$ mm, $\gamma = 0.5$ mm, $\varepsilon_x = 0.45$ mm, $\varepsilon_y = 0.05$ mm and $\Delta_x = \Delta_y = 0.04$ mm; (a) theoretical and (b) experimental.

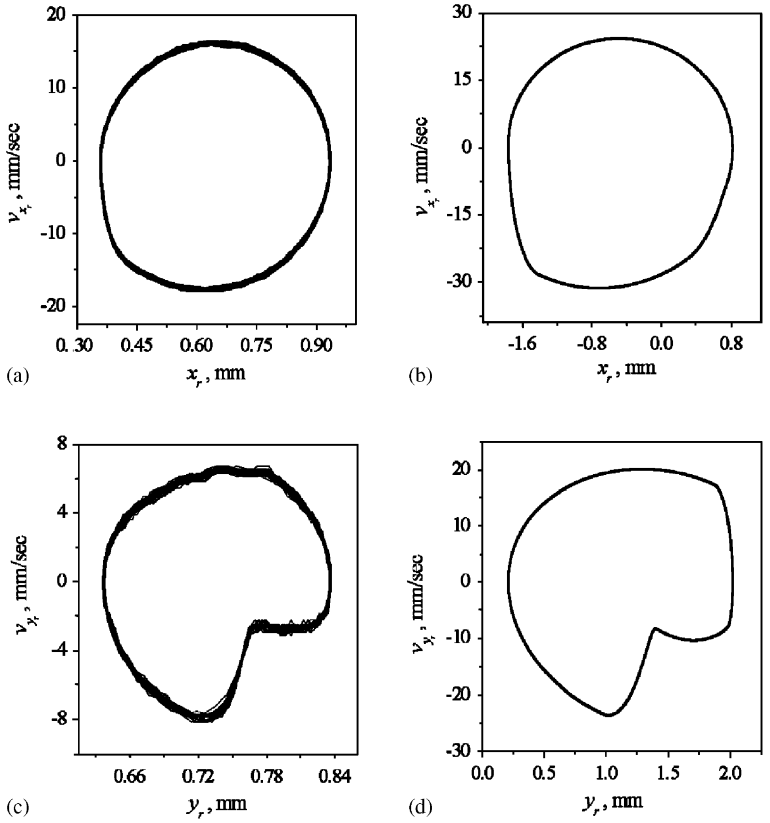

Fig. 7. (a),(c) Experimental and (b),(d) theoretical phase portraits for periodic behaviour of the Jeffcott rotor system in x- and y-directions for the cross-section $f = 13.1$ Hz.

Furthermore, phase portraits in the x and y directions for periodic and chaotic trajectories are examined at $f = 13.1$ and 18.5 Hz in Figs. 7 and 8. The experimental phase portraits in the x- and y-directions are plotted in (a) and (c), and the corresponding to them theoretical graphs are depicted in (b) and (d). As can be seen, again the theoretical predictions correspond well to the experimental results.

Comparing the system responses for different values of the forcing frequency in Figs. 5 and 6, it is clear from the bifurcation diagrams and phase planes that periodic regimes dominate at low and at high frequencies, and chaotic motion occurs in between. The periodic regimes for the low frequency are caused by insufficient excitation of the rotor and as a result either there is no contact between the rotor and the snubber ring or just one contact per period. As the forcing frequency is increased, and the amplitude of oscillations rises the impacts between the rotor and the ring become stronger and the system generates chaotic motion. The periodic regimes that are observed for the high frequencies have a wide range and lower amplitude of vibration than chaotic ones. The experimental results for changing forcing frequency shown above correspond well with the theoretical predictions.

4. Conclusions

The main aim of this paper was to assess the correlation between the responses from the theoretical model [18] and the experiments for the rotor system with a preloaded snubber ring, and to obtain an overview of the global system dynamics, which can be used subsequently to suppress the rotor vibration. More specifically, the experimental verification of a nonlinear Jeffcott rotor model with a preloaded snubber ring has been carried out. The mathematical model neglects frictional and gyroscopic forces, and focuses on the dynamic interactions between a whirling rotor and a preloaded snubber ring having much larger stiffness than the

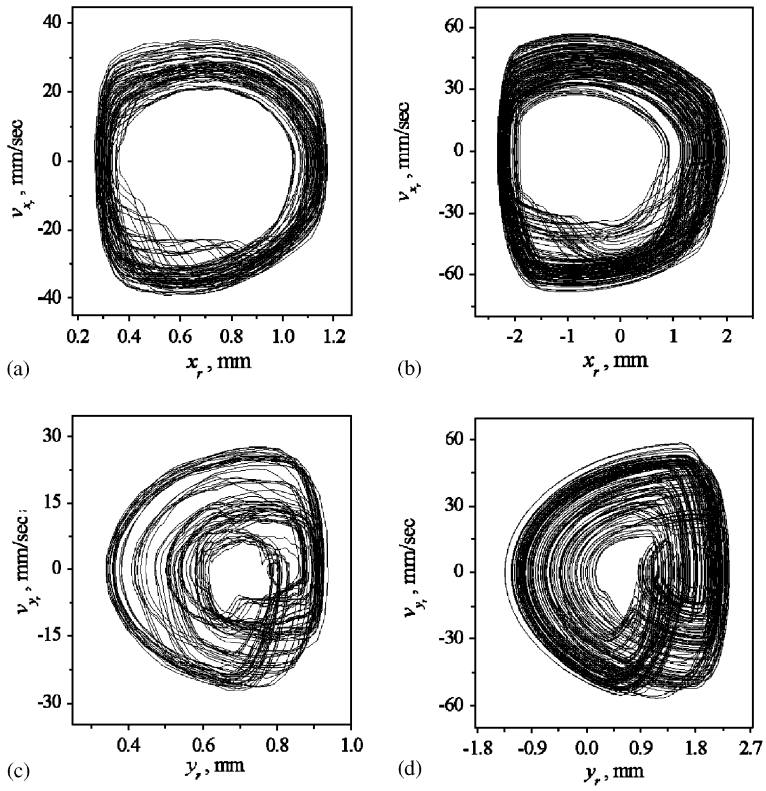

Fig. 8. (a),(c) Experimental and (b),(d) theoretical phase portraits for chaotical behaviour of the Jeffcott rotor system in x- and y-directions for the cross-section $f = 18.5$ Hz.

rotor. The nonlinearity, in the form of a discontinuous stiffness, is caused by the radial clearance between rotor and the snubber ring. The rotor is placed eccentrically within the snubber ring and the eccentricity can be varied.

Theoretical results obtained from analytical approximate solutions and from the direct numerical integration have been verified by the experimental study conducted on a dedicated experimental rig. A detailed description of the experimental rig and the data acquisition system developed are presented, along with the experimental procedures used to investigate the dynamical responses of the system. The results concentrate on the dynamic responses caused by interactions between the whirling rotor and the massless snubber ring having much higher support stiffness than the rotor. Bifurcation diagrams with forcing frequency as a control parameter, Poincaré maps and phase plane diagrams have been used to compare the results obtained from the experiment and the theory. It is clearly shown that the experimental studies have confirmed the basic bifurcation scenarios predicted theoretically for a wide range of system parameters. In conclusion, a good correlation between the experimental and theoretical results has been found.

Acknowledgement

The financial support provided by EPSRC, Rolls-Royce plc and ORS Award Scheme is gratefully acknowledged.

References

[1] M. Wiercigroch, B. de Kraker (Eds.), *Applied Nonlinear Dynamics and Chaos of Mechanical Systems with Discontinuties*, World Scientific, Singapore, 2000.

[2] M.I Feigin, *Forced Oscillations in Systems with Discontinuous Nonlinearities*, Nauka, Moscow, 1994.

[3] F.K. Choy, J. Padovan, Non-linear transient analysis of rotor-casing rub events, *Journal of Sound and Vibration* 113 (1987) 529–545.
[4] A. Muszynska, P. Goldman, Chaotic responses of unbalanced rotor/bearing/stator systems with looseness or rubs, *Chaos, Solitons & Fractals* 5 (1995) 1683–1704.
[5] D.W. Childs, Fractional-frequency rotor motion due to non-symmetric clearance effects, *Transactions of the ASME—Journal of Engineering for Power* 104 (1982) 533–541.
[6] F. Chu, Z. Zhang, Bifurcation and chaos in a rub-impact Jeffcott rotor system, *Journal of Sound and Vibration* 210 (1998) 1–18.
[7] F. Chu, Z. Zhang, Periodic, quasi-periodic and chaotic vibrations of a rub-impact rotor system supported on oil film bearing, *International Journal of Engineering Sciences* 35 (1997) 963–973.
[8] F.F. Ehrich, Spontaneous sidebanding in high-speed rotordynamics, *Transactions of ASME—Journal of Vibration and Acoustics* 114 (1992) 498–505.
[9] R. Ganesan, Dynamic response and stability of a rotor-support system with non-symmetric bearing clearances, *Mechanism Machine Theory* 31 (1996) 781–798.
[10] G. von Groll, D.J. Ewins, A mechanism of low subharmonic response in rotor/stator contact—measurements and simulations, *Transactions of ASME—Journal of Vibration and Acoustics* 124 (2002) 350–358.
[11] H. Diken, Non-linear vibration analysis and subharmonic whirl frequencies of the Jeffcott rotor model, *Journal of Sound and Vibration* 243 (2001) 117–125.
[12] Q. Ding, Hopf bifurcation analysis of a rotor/seal system, *Journal of Sound and Vibration* 252 (2002) 817–833.
[13] E.V. Karpenko, M. Wiercigroch, M.P. Cartmell, Regular and chaotic dynamics of a discontinuously nonlinear rotor system, *Chaos, Solitons & Fractals* 13 (2002) 1231–1242.
[14] E.V. Karpenko, E.E. Pavlovskaia, M. Wiercigroch, Bifurcation analysis of a preloaded Jeffcott rotor, *Chaos, Solitons & Fractals* 15 (2003) 407–416.
[15] D.H. Gonsalves, R.D. Neilson, A.D.S. Barr, A study of response of a discontinuously nonlinear rotor system, *Nonlinear Dynamics* 7 (1995) 451–470.
[16] R.D. Brown, G. Drummond, P.S. Addison, Chaotic response of a short journal bearing, *Proceedings of Institution of Mechanical Engineers—Part J* 214 (2000) 387–400.
[17] R.D. Brown, P. Addison, A.H.C. Chan, Chaos in the unbalance response of journal bearings, *Nonlinear Dynamics* 5 (1994) 421–432.
[18] E.E. Pavlovskaia, E.V. Karpenko, M. Wiercigroch, Nonlinear dynamics of a Jeffcott rotor with a preloaded snubber ring, *Journal of Sound and Vibration* 276 (1–2) (2004) 361–379.
[19] M. Wiercigroch, Control of vibration by smart SMA-embedded composite structures, Final Report to EPSRC, 2003.